Delft University of Technology

Document Version
Final published version

Licence
Dutch Copyright Act (Article 25fa)

Citation (APA)
Green, E. R., Negretti, N. M., Shealy, N. G., Moser, F. A., Lehmann, C. J., Byndloss, M. X., van de Plas, R., Zackular, J. P., Skaar, E. P., & More Authors (2026). The intestinal microbiota impacts nutritional immunity and resistance to Acinetobacter baumannii pneumonia. *Proceedings of the National Academy of Sciences of the United States of America*, *123*(17), Article e2534432123. https://doi.org/10.1073/pnas.2534432123

Important note
To cite this publication, please use the final published version (if applicable).
Please check the document version above.

Copyright
In case the licence states “Dutch Copyright Act (Article 25fa)”, this publication was made available Green Open Access via the TU Delft Institutional Repository pursuant to Dutch Copyright Act (Article 25fa, the Taverne amendment). This provision does not affect copyright ownership.
Unless copyright is transferred by contract or statute, it remains with the copyright holder.

Sharing and reuse
Other than for strictly personal use, it is not permitted to download, forward or distribute the text or part of it, without the consent of the author(s) and/or copyright holder(s), unless the work is under an open content license such as Creative Commons.

Takedown policy
Please contact us and provide details if you believe this document breaches copyrights.
We will remove access to the work immediately and investigate your claim.

This work is downloaded from Delft University of Technology.

SEE CORRECTION FOR THIS ARTICLE

MICROBIOLOGY

The intestinal microbiota impacts nutritional immunity and resistance to *Acinetobacter baumannii* pneumonia

Erin R. Green[a,1], Nicholas M. Negretti[b,c], Tess H. Brunner[a,d], Nicolas G. Shealy[e,f,g,h], Felipe A. Moser[i], Sydney L. Drury[e,f], Kacie A. Traina[e,f], Valeria M. Reyes Ruiz[e,f], Tzushan S. Yang[e], Christopher J. Lehmann[d,j], Mariana X. Byndloss[e,f,k], Raf Van de Plas[i,l,m], Joseph P. Zackular[g,h,n], Samuel H. Light[a,d], Jennifer M. S. Sucre[b,c,o], and Eric P. Skaar[e,f,1]

Affiliations are included on p. 10.

Contributed by Eric P. Skaar; received November 26, 2025; accepted March 20, 2026; reviewed by Alison K. Criss and Amanda G. Oglesby

Broad-spectrum antibiotics are frequently administered to intensive care unit patients as part of empiric care. This treatment has been associated with subsequent infections by the emerging nosocomial pathogen *Acinetobacter baumannii*; however, the mechanisms underlying this linkage remain unclear. Here, we observe an association between antibiotic treatment and microbiota disruption that precedes *A. baumannii* infection in a hospitalized patient cohort and demonstrate in a murine model that broad-spectrum antibiotic administration drives susceptibility to intranasal infection with this pathogen. Reconstitution of the intestinal microbiota by fecal microbiota transplant restores control of *A. baumannii* bloodstream dissemination, implicating microbiota dysbiosis as a key driver of pulmonary disease. Using single-cell RNA sequencing, we determine that antibiotic pretreatment reduces the abundance of transcripts related to phagocyte effector functions in the lung, including nutritional immunity pathways that restrict pathogen access to essential nutrient metals. Depletion studies identify neutrophils and inflammatory monocytes as central mediators of microbiota-dependent protection, and loss of the nutritional immunity components lipocalin-2 or calprotectin abrogates the effects of antibiotics on infected mice, demonstrating a causal relationship between microbiota dysbiosis and impaired phagocyte-mediated nutritional immunity. Together, these findings provide a mechanism for the increased severity of *A. baumannii* pneumonia following antibiotic exposure and highlight the intestinal microbiota as a potential therapeutic target to prevent nosocomial infections with this and other healthcare-associated pathogens.

Acinetobacter baumannii | nutritional immunity | microbiota | gut–lung axis | nosocomial infections

Significance

Antibiotics are routinely administered to critically ill hospital patients to treat infection. However, antibiotic treatment is often associated with subsequent healthcare-associated infections, including pneumonias caused by the emerging nosocomial pathogen *Acinetobacter baumannii*. Here, we show that broad-spectrum antibiotic administration disrupts the intestinal microbiota and suppresses the expression of pulmonary phagocyte pathways that sequester nutrient metals in the lung. This loss of microbiota-dependent nutritional immunity enhances *A. baumannii* dissemination, resulting in more severe disease. Restoring a healthy microbiota reinstates control of systemic infection, revealing a gut–lung connection that influences susceptibility to this pathogen. These findings identify a mechanism by which antibiotic exposure exacerbates *A. baumannii* pneumonia severity and highlight the potential of microbiota-targeted strategies to prevent healthcare-associated infections with this pathogen.

The gram-negative bacterial pathogen *Acinetobacter baumannii* is recognized as an urgent public health threat due to its multidrug resistance, persistence in the hospital environment, and association with high rates of mortality in critically ill patients (1–4). Despite the rising prevalence of community-acquired *A. baumannii* infections (5, 6), the majority of infections occur in healthcare settings, where it is an emerging cause of nosocomial pneumonias, including ventilator-associated pneumonias (1, 7, 8). Critically ill patients in intensive care units (ICUs) and those receiving mechanical ventilation are at high risk for *A. baumannii* infection (9, 10). However, additional points of vulnerability for *A. baumannii* transmissions and risk factors driving poor disease outcomes among hospitalized patients have not been well defined.

Broad-spectrum antibiotics are widely administered in ICUs, with some reports estimating that up to 71% of ICU patients receive antibiotics (11–13), frequently as part of standard empiric therapy that precedes infection diagnosis (14). As a result, ICU patients often exhibit marked dysbiosis of their intestinal microbiota, which has been associated with an increased risk of adverse outcomes, including healthcare-associated infections (15–18). Clinical and murine studies have consistently linked antibiotic administration with an increased risk of infection by a spectrum of nosocomial pathogens in the intestinal tract (19–21). This association is traditionally attributed to antibiotic-mediated disruption of colonization resistance, the mechanism by which the normal microbiota suppresses pathogen colonization and overgrowth within the intestinal compartment (22, 23). Additionally, antibiotic administration has been associated with infections by pathogens at extraintestinal systemic tissue sites, including viral, fungal, and bacterial pathogens in the lung (24–28). In these instances, increased susceptibility to infection is hypothesized to be driven by aberrant crosstalk between the gut and immune system, leading to a dysregulated and impaired systemic immune response (29–32). However, the mechanisms by which antibiotic-driven changes in the gut microbiota impact systemic immune

Reviewers: A.K.C., University of Virginia; and A.G.O., University of Maryland Baltimore.

The authors declare no competing interest.

Copyright © 2026 the Author(s). Published by PNAS. This article is distributed under Creative Commons Attribution-NonCommercial-NoDerivatives License 4.0 (CC BY-NC-ND).

[1]To whom correspondence may be addressed. Email: eringreen@uchicago.edu or eric.skaar@vumc.org.

This article contains supporting information online at https://www.pnas.org/lookup/suppl/doi:10.1073/pnas.2534432123/-/DCSupplemental.

Published April 21, 2026.

Downloaded from https://www.pnas.org by TU DELFT BIBLIOTHEEK on October 22, 2026 from IP address 131.180.130.24.

responses, and the consequences of this crosstalk on infection control, are not completely understood.

Antimicrobial therapy has been associated with incidences of *A. baumannii* infection and poor disease outcomes within hospital settings, suggesting that antibiotic exposure may impact susceptibility to infections with this pathogen (33–41). However, whether prior antibiotic administration directly drives *A. baumannii* infection severity is not known. Here, we use a murine model to demonstrate that antibiotic-mediated disruption of the gut microbiota is a direct driver of susceptibility to respiratory infection with this pathogen. Additionally, we show that antibiotic administration dampens the expression of neutrophil effector functions in the lung, leading to a suppression of nutritional immunity and enhanced *A. baumannii* dissemination. Together, these findings provide insight into the mechanisms underlying the clinical association between antibiotic exposure and *A. baumannii* infection and highlight the importance of microbiota-immune crosstalk in the control of respiratory infections with this pathogen.

Results

Antibiotic Therapy and Gut Microbiome Dysbiosis Precede *Acinetobacter* Infection in Hospitalized Patients. To investigate clinical associations between antibiotic exposure, gut microbiome composition, and *Acinetobacter* infection, we analyzed data from multiple prospective observational cohort studies that collected fecal microbiome data from patients admitted to The University of Chicago Medical Center (UCM) (16, 42–47). The total cohort included in our analysis contained 1,275 hospitalized patients from high-risk groups for healthcare-associated *Acinetobacter* infections, including liver or heart transplant recipients, liver disease patients, and medical intensive care unit (MICU) patients (*SI Appendix*, Fig. S1*A*). Review of patient medical history records identified 18 independent *Acinetobacter* infections (defined as clinical tests with *Acinetobacter*-positive cultures) within our patient cohort (*SI Appendix*, Fig. S1*A*), with respiratory tract isolates (12/18) associated with pneumonia or ventilator-associated pneumonia (VAP) diagnoses accounting for the majority of infections (Fig. 1*A*, *SI Appendix*, Fig. S1*B*, and Dataset S1).

Of the 18 identified *Acinetobacter* infections, review of patient medical history records revealed 11 instances of antibiotic exposure within the preceding 30 d, including in 10/12 pneumonia or VAP diagnoses (Fig. 1*B*, *SI Appendix*, Fig. S1*A*, and Dataset S1). Further analysis of five patients with fecal samples collected within 30 d preceding *Acinetobacter* infections revealed pre-*Acinetobacter* infection microbiomes that exhibited substantially altered microbial community structures relative to healthy controls (Fig. 1 *C* and *D* and *SI Appendix*, Fig. S1*C*). Notably, all five of these patients received antimicrobial therapy within 30 d prior to *Acinetobacter* culture (*SI Appendix*, Fig. S1*C*). The pre-*Acinetobacter* infection microbiomes displayed common features of antibiotic-induced dysbiosis, including a marked reduction in diversity and expansion of *Enterococcus faecium* in two patients (Fig. 1 *C* and *E*). Together, these findings are consistent with a temporal relationship wherein antibiotic treatment and microbiome dysbiosis precede *Acinetobacter* infection in hospitalized patients.

Broad-Spectrum Antibiotic Administration Increases Susceptibility to *A. baumannii* Pneumonia in a Murine Model. To mechanistically assess the impact of antibiotic treatment on susceptibility to respiratory infections with *A. baumannii*, a murine model of *A. baumannii* pneumonia was employed. Mice were administered a cocktail of broad-spectrum antibiotics (ampicillin, vancomycin, and gentamicin) in drinking water

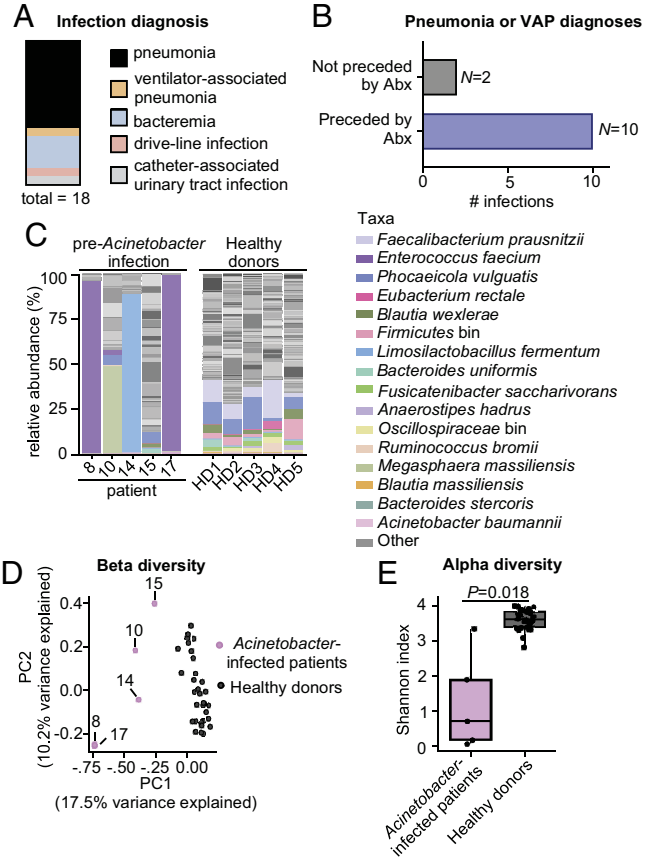

Fig. 1. Antibiotic treatment and microbiome dysbiosis precede *Acinetobacter* infection in hospitalized patients. (*A*) Infection types associated with *Acinetobacter*-positive cultures among hospitalized patients from UCM prospective cohort studies. *N* = 18. (*B*) Proportion of respiratory tract *Acinetobacter* infections preceded by antibiotic administration (Abx) within the 30 d prior to positive clinical culture. *N* = 12. (*C*) Taxonomic composition of fecal microbiomes determined by shotgun metagenomic sequencing, comparing samples from patients prior to *Acinetobacter* infection with representative healthy donor controls. Detailed timelines of antibiotic administration and sample collection for these patients are provided in *SI Appendix*, Fig. S1. (*D*) Beta diversity analysis using principal coordinate analysis of microbial community structures comparing preinfection patient samples and healthy controls. Patient identifiers correspond to samples shown in panel *C*. (*E*) Alpha diversity analysis comparing preinfection patient samples and healthy controls, quantified using Shannon diversity index. Statistical significance determined by Student's *t* test.

for 5 d, then were intranasally infected with *A. baumannii* 2 d after cessation of antibiotics (Fig. 2*A*). Mice administered antibiotics exhibited weight loss over the course of treatment (*SI Appendix*, Fig. S2 *A* and *B*), consistent with reports of oral antibiotic administration in murine models causing dehydration and malnutrition that can suppress weight gain (48, 49). Prior studies have demonstrated that antibiotic-induced weight loss can suppress antibacterial immune responses (48, 49); however, we detected no gross pathological differences in the lungs of control and antibiotic-treatment groups in the absence of infection (*SI Appendix*, Fig. S2 *C*–*F*). Upon intranasal inoculation with *A. baumannii*, the antibiotic-treated group exhibited a higher rate of mortality (Fig. 2*B*) than control animals, which was associated with increased weight loss (*SI Appendix*, Fig. S2*B*), a significant increase in bacterial colonization of the lungs (Fig. 2*C*), and higher levels of dissemination to the liver and spleen (Fig. 2 *D* and *E*). Histopathological examination of infected lungs (Fig. 2*F*) revealed that mice that received antibiotics prior to infection exhibited decreased alveolar inflammation (Fig. 2*G*) and edema

Downloaded from https://www.pnas.org by TU DELFT BIBLIOTHEEK on October 22, 2026 from IP address 131.180.130.24.

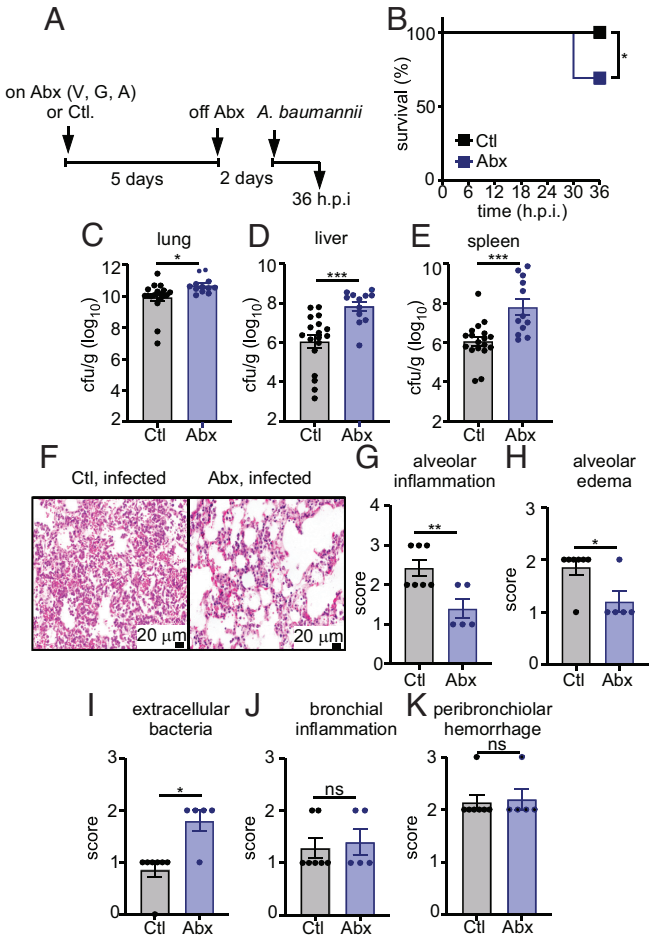

Fig. 2. Broad-spectrum antibiotic administration increases susceptibility to *A. baumannii* pneumonia in a murine model. (*A*) Mice were administered a cocktail of ampicillin (A), gentamicin (G), and vancomycin (V), or a vehicle control, in their drinking water for 5 d. Water was removed for 48 h and mice were infected with 4×10^8 CFUs of *A. baumannii* via intranasal inoculation. (*B*) Survival following intranasal infection of antibiotic-treated (Abx) and control (Ctl) mice with *A. baumannii*. (N = 12-13). (*C–E*) Bacterial burdens in the indicated tissues 36 h.p.i. of Abx and control mice. Data are mean ± SEM. (N = 12-18). (*F*) Histology by H&E staining at 36 h.p.i. in the lungs of Abx and Ctl mice. (*G–K*) Pathology scores assessing alveolar inflammation (*G*), alveolar edema (*H*), extracellular bacteria (*I*), bronchial inflammation (*J*), and peribronchiolar hemorrhage (*K*) in the lungs of Abx and Ctl mice at 36 h.p.i. Data are mean ± SEM. (N = 6). Panel *B* by the log-rank Mantel-Cox test. Panels *C–E* by Student's t test on $\log_{10}$-transformed data. Panels *G–K* by Student's t test. $^*P < 0.05$, $^{**}P < 0.01$, $^{***}P < 0.001$, ns = not significant.

(Fig. 2*H*), despite harboring increased levels of extracellular bacteria in the alveolus (Fig. 2*I*). These findings demonstrate an association between a dampened acute inflammatory response and accumulation of extracellular bacteria in the antibiotic-treated group. By contrast, no differences in bronchial inflammation (Fig. 2*J*) or peribronchiolar hemorrhage (Fig. 2*K*) were detected between the two groups. Together, these data demonstrate that broad-spectrum antibiotic exposure drives susceptibility to *A. baumannii* infection and establish an experimental framework for elucidating the molecular mechanisms driving this association.

Disruption of the Intestinal Microbiota by Antibiotics Drives Enhanced Mortality and Bacterial Dissemination Following *A. baumannii* Pneumonia. Previous studies have demonstrated a connection between disruption of the gastrointestinal microbiota by broad-spectrum antibiotic administration and the severity of lung-related diseases, including susceptibility to respiratory infections by bacterial and viral pathogens (24, 26–28, 30, 50). Additionally, in clinical cohort studies we observed that *Acinetobacter*-infected patients displayed a marked decrease in preinfection microbiome diversity relative to healthy donor controls (Fig. 1*E*). To assess whether disruption of the intestinal microbiota drives antibiotic-dependent increases in *A. baumannii* lung colonization and dissemination in a murine model, fecal microbiota transplants (FMTs) were performed using the stool of control-group animals as a donor (Fig. 3*A*). We observed that FMT had no impact on control of lung burdens (Fig. 3*B*), but restored the ability of antibiotic-treated mice to restrict bacterial dissemination to the liver (Fig. 3*C*) and spleen (Fig. 3*D*). Additionally, while administration of FMT lengthened the postantibiotic exposure period by 2 d (Fig. 3*A*), animals that previously received antibiotics exhibited a sustained decrease in weight relative to vehicle control mice at the time of infection, regardless of FMT treatment (*SI Appendix*, Fig. S3*A*). These data suggest that phenotypes observed after FMT resulted from microbiota restoration, rather than recovery from antibiotic-induced weight loss. Together, these findings imply that disruption of the intestinal microbiota by broad-spectrum antibiotics enhances bacterial dissemination from the lung and/or bacterial replication in deep tissue sites.

To determine how differential changes in the gut microbiota might impact *A. baumannii* disease outcomes, we next administered seven different antibiotic combinations in our antibiotic pretreatment model (Fig. 3*E*) and monitored survival and bacterial loads following *A. baumannii* intranasal infection in each group. More specifically, groups of mice were treated with either no antibiotic, vancomycin, gentamicin, or ampicillin individually, in each pairwise combination, or with a cocktail of all three drugs. These combinations were chosen to interrogate whether administration of a single antibiotic or pairwise combination was sufficient to drive susceptibility to pneumonia. We found that mice receiving vancomycin in their drinking water in any combination exhibited a survival defect (Fig. 3*F*) that was almost always associated with enhanced bacterial burdens in the liver and spleen (Fig. 3 *G–I*), suggesting that administration of vancomycin in the drinking water is sufficient to enhance *A. baumannii* infection severity in a pneumonia model. Additionally, we observed a similar association between antibiotic treatment and disease outcome when mice were treated with ampicillin and gentamicin in combination (Fig. 3 *F–I*).

To delineate microbial taxa associated with either control of, or susceptibility to, *A. baumannii* pneumonia, fecal pellets were collected from all treatment groups before antibiotic administration and immediately prior to infection and subjected to 16S rRNA gene sequencing. 16S sequencing revealed that the different antibiotic treatment combinations created distinct community structures (Fig. 3*J* and *SI Appendix*, Fig. S3 *B–D*), which is consistent with the variation observed in the ability of each group to control infection and prevent bloodstream dissemination. Moreover, mice receiving vancomycin as part of their antibiotic treatment, or treated with ampicillin and gentamicin in combination, showed a specific expansion of *Enterobacteriaceae* family representatives in their fecal pellets (Fig. 3*J*), suggesting that changes in the abundance of these taxa may be associated with differential disease outcomes. Additionally, depletion of *Bacteroidaceae* family members was observed when mice were treated with vancomycin and ampicillin in combination, or with a cocktail of all three antibiotics (Fig. 3*J*). Upon assessing putative associations between the relative abundance of these bacterial taxa in fecal pellets and the tissue burden of *A. baumannii* after infection (Fig. 3 *K* and *L* and *SI Appendix*, Fig. S3 *E–H*), we identified a statistically significant positive correlation between the abundance of *Enterobacteriaceae* in the feces and *A. baumannii*

Downloaded from https://www.pnas.org by TU DELFT BIBLIOTHEEK on October 22, 2026 from IP address 131.180.130.24.

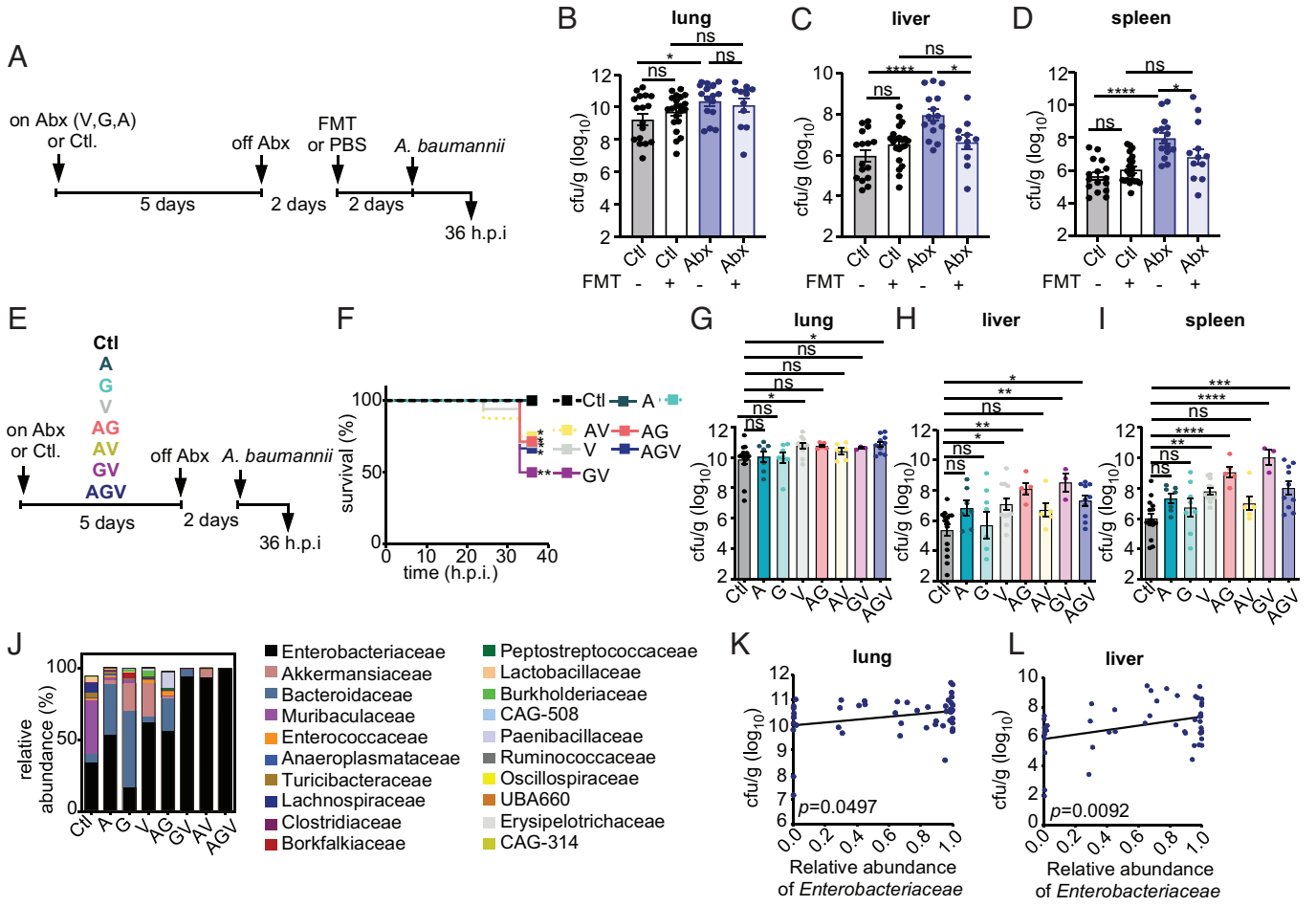

Fig. 3. Disruption of the intestinal microbiota by antibiotics drives enhanced mortality and bacterial dissemination following *A. baumannii* pneumonia. (*A*) 48 h after the completion of antibiotic cocktail (vancomycin, ampicillin, gentamicin) treatment (Abx), mice were subjected to FMT with untreated donor stool or vehicle control (PBS). After 48 h of FMT engraftment, *A. baumannii* was administered intranasally. (*B–D*) Bacterial burdens in the indicated tissues at 36 h.p.i. of Abx and control (Ctl) mice subjected to FMT. Data are mean ± SEM. (*N* = 11-21). (*E*) Individual or combinatorial doses of ampicillin (A), gentamicin (G), or vancomycin (V) were supplemented in the drinking water of mice for 5 d. Water was removed for 48 h and mice were administered *A. baumannii* via intranasal infection. (*F*) Survival following *A. baumannii* intranasal infection. (*N* = 6-14). (*G–I*) Bacterial burdens in the indicated tissues of Abx and Ctl mice at 36 h.p.i. Data are mean ± SEM. (*N* = 3-10). (*J*) 16S rRNA profiling of bacterial communities from the indicated antibiotic treatment groups at the family level. (*N* = 3-10). (*K* and *L*) Correlation analysis of relative abundance of *Enterobacteriaceae* in the gut microbiota after Abx treatment with *A. baumannii* bacterial burdens in the indicated tissues at 36 h.p.i. (*N* = 48). Panels *B–D* by One-Way ANOVA with Šidák's multiple comparison post-test. Panel *F* by the Log-Rank Mantel-Cox test relative to control group. Panels *G–I* by One-Way ANOVA with Dunnett's multiple comparison post-test. Panels *K* and *L* by linear regression. **P* < 0.05, ***P* < 0.01, ****P* < 0.001, *****P* < 0.0001, ns = not significant.

colonization of the lung (Fig. 3*K*) and liver (Fig. 3*L*). Together, these data suggest that disruption of the normal microbiota by broad-spectrum antibiotics, which is associated with a bloom in *Enterobacteriaceae*, promotes the bloodstream dissemination of *A. baumannii* during respiratory infection.

Antibiotic Administration Dampens Innate Immune Activation during *A. baumannii* Pneumonia. Previous studies have demonstrated a role for the gut microbiota in regulating the development and priming of systemic immune responses (51–54). To interrogate the impact of antibiotic treatment on the immune response to *A. baumannii* pneumonia, single-cell RNA-sequencing (scRNA-seq) was performed on $CD45^+$ immune cells isolated from the lungs of mice treated with a cocktail of vancomycin, gentamicin, and ampicillin prior to infection and a control group of mice, with tissues processed for sequencing from uninfected controls and after 36 h of *A. baumannii* infection (Fig. 4*A*). Unsupervised clustering of the dataset was performed (Dataset S2), and cell types were assigned to each cluster based on the relative expression of cell-type-specific marker genes (*SI Appendix*, Fig. S4*A*). This analysis identified the expected immune cell populations, including neutrophils, monocytes, alveolar and interstitial macrophages, as well as B, T, and Natural Killer cell subsets (Fig. 4*B*, *SI Appendix*, Fig. S4*A*, and Dataset S3). Consistent with previous reports (55–59), we detected a large increase in the population of myeloid cells, including neutrophils, monocytes, and type I and II dendritic cells, within the lung following establishment of *A. baumannii* infection (Fig. 4 *C* and *E*). However, no substantial differences in the overall immune cell clustering (Fig. 4*D*) or abundance of cell-type populations (Fig. 4*E*) were observed when comparing control and antibiotic-treated groups. We therefore hypothesized that differential activation of immune cell pathways, rather than changes in immune cell abundance or recruitment, could be driving differences in susceptibility between control and antibiotic-treated mice.

To identify potential differences in immune pathway activation, gene ontology enrichment analysis was performed on genes showing differential expression (≥0.25 or ≤–0.25 Log_2 fold-change) in the total lung immune cell population of the antibiotic-treated group relative to the control group after infection (Fig. 4*F*, *SI Appendix*, Fig. S4*B*, and Dataset S4). Among the genes showing decreased expression in the antibiotic-treated group, we detected an enrichment in transcripts involved in several innate immune response pathways, including

Downloaded from https://www.pnas.org by TU DELFT BIBLIOTHEEK on October 22, 2026 from IP address 131.180.130.24.

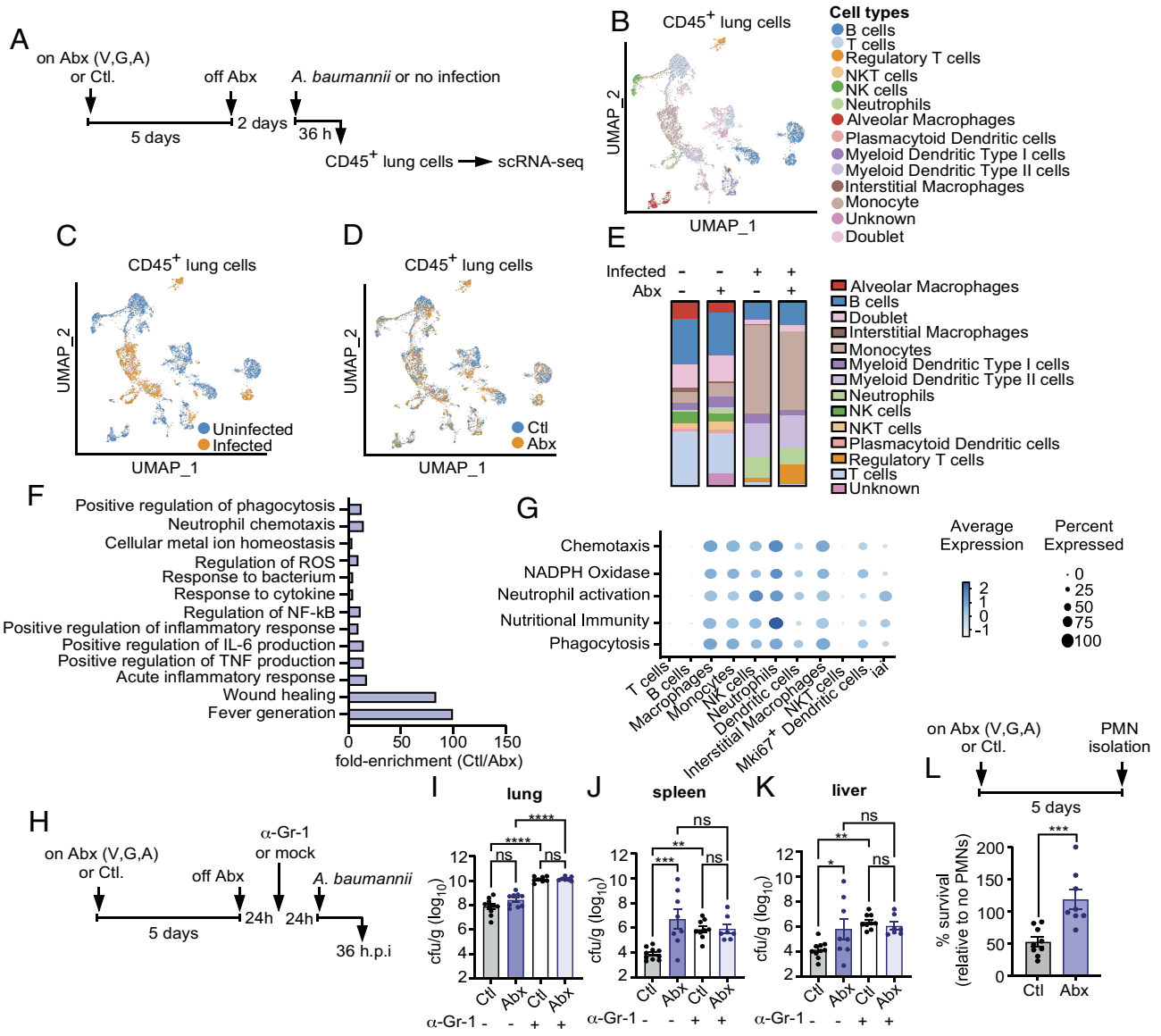

Fig. 4. scRNA-seq reveals a blunted signature of neutrophil activation in the lungs of mice treated with vancomycin, gentamicin, and ampicillin prior to infection. (*A*) 48 h after the completion of antibiotic cocktail (vancomycin, gentamicin, and ampicillin) treatment (Abx) or control treatment (Ctl), *A. baumannii* was administered intranasally. At 36 h.p.i., lungs were isolated, and CD45$^+$ cells were analyzed by scRNA-seq. (*B*) UMAP representation of all CD45$^+$ cell clusters in scRNA-seq data from the lungs of Ctl and Abx-treated mice ± infection with *A. baumannii* ($N = 4$ per group). (*C* and *D*) UMAP representation of infection status (*C*) and antibiotic treatment (*D*) in all CD45$^+$ cell lung clusters. (*E*) Relative abundance of different CD45$^+$ scRNA-seq cell populations across infection and treatment groups. (*F*) Gene ontology enrichment analysis of genes showing higher (≥0.25 $\log_2$FC) expression in the total lung cells of *A. baumannii*–infected Ctl mice relative to those of Abx-treated mice. (*G*) Relative expression of innate immune gene sets across CD45$^+$ lung cell types. (*H*) anti-Gr-1 cell-depleting antibody (α-Gr-1) or a mock treatment was administered intraperitoneally to Abx and Ctl groups 24 h before intranasal inoculation with *A. baumannii*. (*I*–*K*) CFUs recovered at 36 h.p.i. from the indicated tissues of neutrophil- and monocyte-depleted (α-Gr-1) mice in Abx and Ctl groups. Data are mean ± SEM. ($N = 7$-10). (*L*) Recovery of *A. baumannii* after 2 h of incubation at a multiplicity of infection of 0.025 with neutrophils isolated from the bone marrow of Ctl or Abx mice, relative to a media-only control. Data are mean ± SEM. ($N = 8$-9). Panels *I*–*K* by One-Way ANOVA with Šidák's multiple comparison post-test. Panel *L* by Student's *t* test. *$P < 0.05$, **$P < 0.01$, ***$P < 0.001$, ****$P < 0.0001$, ns = not significant.

neutrophil chemotaxis, regulation of ROS production, phagocytosis, and other signatures of phagocyte activation (Fig. 4*F*). Across all treatment groups, expression of gene sets related to these pathways was most abundant in neutrophil, monocyte, and macrophage subsets (Fig. 4*G*), suggesting that dysregulation or decreased activation of these cell types in antibiotic-treated mice might be driving susceptibility to infection.

To investigate the impact of monocytes and neutrophils on antibiotic-mediated susceptibility to infection, inflammatory monocytes and neutrophils were depleted prior to infection. Depletions were performed using the RB6-8C5 antibody (Fig. 4*H*), which recognizes the Gr-1 epitope present on Ly6G and Ly6C, markers of neutrophils and inflammatory monocytes, respectively (60). Consistent with previous reports (56, 61), we found that neutrophil and inflammatory monocyte depletion increased *A. baumannii* lung colonization and dissemination to the spleen and liver (Fig. 4 *I*–*K*). However, no differences in lung burdens or bacterial dissemination were observed when comparing control- and antibiotic-treated groups depleted of neutrophils and inflammatory monocytes (Fig. 4 *I*–*K*), suggesting that these cell types may be driving the differences in susceptibility between the two groups. Moreover, neutrophils isolated from the bone marrow of antibiotic-treated mice exhibited reduced killing of *A. baumannii* in vitro (Fig. 4*L*), indicating that antibiotic treatment inhibits the antibacterial function of these cells. Additionally, we observed no significant differences in the recruitment of Ly6G$^+$ neutrophils

Downloaded from https://www.pnas.org by TU DELFT BIBLIOTHEEK on October 22, 2026 from IP address 131.180.130.24.

to the lungs of control and antibiotic-treated mice after infection (*SI Appendix*, Fig. S4*C*), further supporting the hypothesis that differences in the activation of neutrophil effector functions, rather than neutrophil abundance, might be driving antibiotic-dependent susceptibility to infection.

Antibiotic Treatment Suppresses Neutrophil-Mediated Nutritional Immunity. To define the impact of antibiotic treatment on neutrophil effector functions, scRNA-seq data were examined for the neutrophil-specific expression of gene sets related to several key antibacterial pathways, including chemotaxis, NADPH oxidase activation, neutrophil activation, nutritional immunity, and phagocytosis (Fig. 5 *A* and *B* and *SI Appendix*, Fig. S5 *A–D*). This comparison revealed that, relative to the control group, neutrophils in the antibiotic-treated group display an aggregate decrease in expression of genes related to NADPH oxidase activation, nutritional immunity, and phagocytosis, suggesting that antibiotic administration impairs the activation or maintenance of these functional pathways in circulating neutrophils.

Nutritional immunity, which involves the sequestration of essential micronutrients from invading pathogens, including the transition metals iron, zinc, and manganese, is elaborated in large part through the effector functions of neutrophils (62, 63) and is a critical component of the innate immune response to *A. baumannii* infection (64–66). The scRNA-seq revealed significant decreases in the expression of several key facets of nutritional immunity in the neutrophils of the antibiotic-treated group relative to those of control animals, including *Hp,* encoding haptoglobin, *Lcn2,* encoding lipocalin-2 (LCN2), and *Ftl1,* encoding ferritin light chain 1 (Fig. 5*B* and Dataset S5). While not reaching statistical significance, decreased expression of *S100a9*, encoding a subunit of calprotectin (CP), and *Ltf*, encoding lactoferrin, was also detected in the antibiotic-treated group (Dataset S5). To validate these observations, RNA fluorescence in situ hybridization (RNA FISH) was performed to measure the abundance and localization of select nutritional immunity transcripts across lung tissues of each infection group (*SI Appendix*, Fig. S6 *A* and *B*). In agreement with the scRNA-seq, we observed strong induction of *Lcn2, Ltf, S100a9,* and *Hp* following *A. baumannii* infection (*SI Appendix*, Fig. S6 *A–F*), consistent with an increase in neutrophil recruitment to the lung after infection (*SI Appendix*, Fig. S4*C*). However, this analysis revealed a trend toward decreased induction

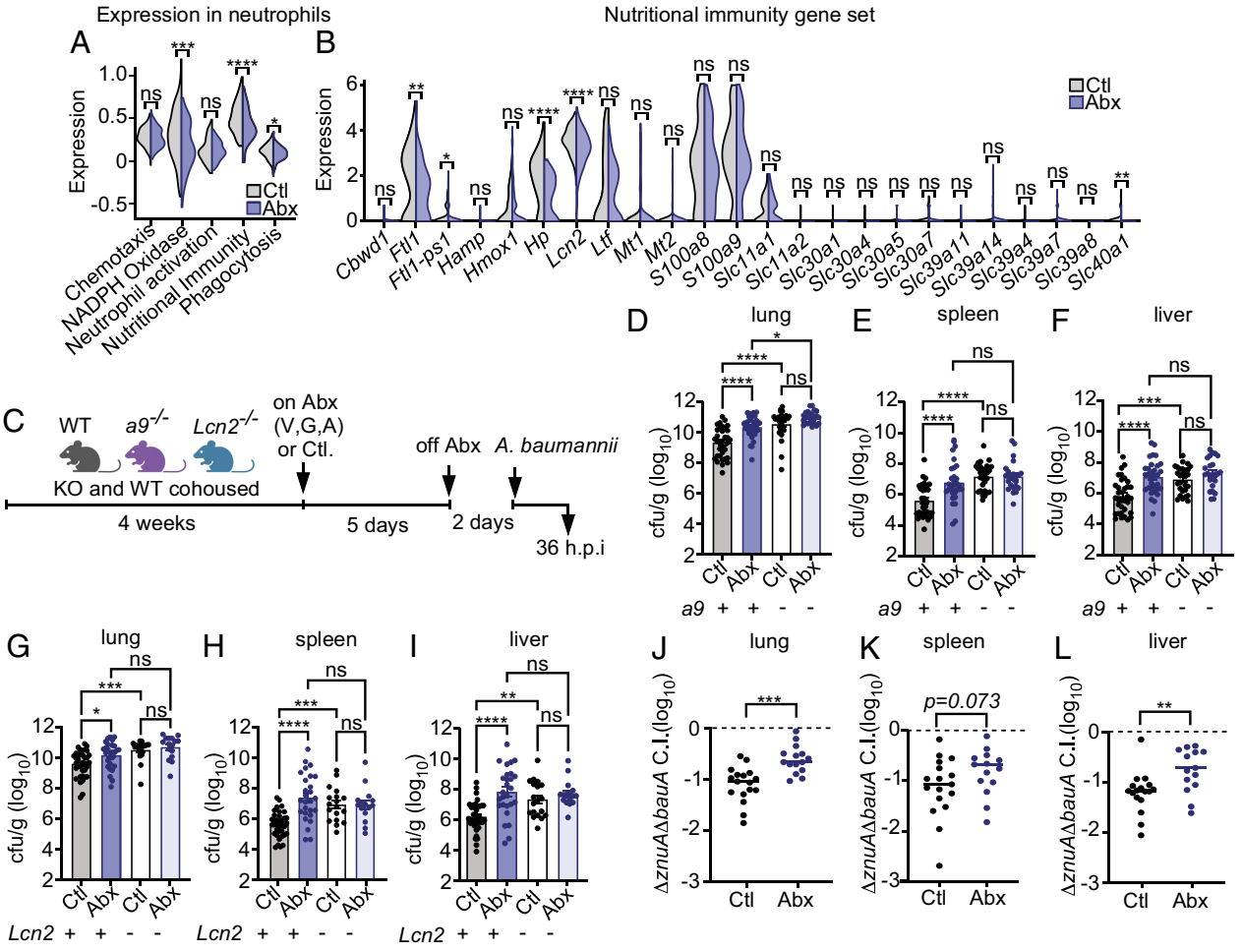

Fig. 5. Administration of vancomycin, gentamicin, and ampicillin reduces nutritional immunity-mediated protection against *A. baumannii* pneumonia. (*A*) Relative expression of innate immune gene sets within the lung neutrophil population after 36 h of *A. baumannii* infection of control (Ctl) mice and mice pretreated with a cocktail of ampicillin, vancomycin, and gentamicin (Abx) ($N = 4$ per group). (*B*) Relative expression of nutritional immunity genes within the lung neutrophil population of Ctl and Abx mice infected with *A. baumannii* for 36 h ($N = 4$ per group). (*C*) 4-wk-old C57BL/6J WT mice were cohoused with age- and sex-matched C57BL/6J *S100a9*$^{-/-}$ (*a9*$^{-/-}$) or C57BL/6J *Lcn2*$^{-/-}$ (*Lcn2*$^{-/-}$) mice for 4 wk. Abx or Ctl water was administered for 5 d, Abx were removed, and mice were infected with *A. baumannii* by intranasal inoculation. (*D–F*) CFUs recovered from the indicated tissues at 36 h.p.i. of WT and *a9*$^{-/-}$ mice in Abx and Ctl groups. Data are mean ± SEM. ($N = 25$-36). (*G–I*) CFUs recovered at 36 h.p.i. from the indicated tissues of WT and *Lcn2*$^{-/-}$ mice in Abx and Ctl groups. Data are mean ± SEM. ($N = 16$-36). (*J–L*) C.I. of Δ*znuA*Δ*bauA* after coinfection with WT *A. baumannii* at 36 h.p.i. in the indicated tissues of Abx and Ctl mouse groups. ($N = 14$-17). Panels *A* and *B* by Student's *t* test. Panels *D–I* by One-Way ANOVA with Šidák's multiple comparison post-test. Panels *J–L* by Student's *t* test on $\log_{10}$-transformed data. $^{*}P < 0.05$, $^{**}P < 0.01$, $^{***}P < 0.001$, $^{****}P < 0.0001$, ns = not significant.

Downloaded from https://www.pnas.org by TU DELFT BIBLIOTHEEK on October 22, 2026 from IP address 131.180.130.24.

of *Lcn2* (*SI Appendix*, Fig. S6*C*), *S100a9* (*SI Appendix*, Fig. S6*E*), and *Hp* (*SI Appendix*, Fig. S6*F*) in the infected, antibiotic-treated group, supporting the conclusions that activation of these factors is diminished following antibiotic treatment.

To evaluate the role of *Lcn2* and *S100a9* in mediating microbiota-dependent protection against *A. baumannii* pneumonia, the virulence of *A. baumannii* was assessed in WT, *S100a9*$^{-/-}$, and *Lcn2*$^{-/-}$ C57BL/6J mice. Prior to infection, WT and knockout mice were cohoused for 4 wk to reduce genotype-dependent differences in microbiota composition (Fig. 5*C*). Following cohousing, mice were subjected to antibiotic administration prior to establishment of intranasal infection (Fig. 5*C*). Consistent with previous reports (64, 65), we observed increased lung colonization and bloodstream dissemination of *A. baumannii* in both *S100a9*$^{-/-}$ (Fig. 5 *D–F*), and *Lcn2*$^{-/-}$(Fig. 5 *G–I*) mice, highlighting the importance of these factors in controlling *A. baumannii* pneumonia. However, antibiotic administration did not exacerbate lung colonization or bloodstream dissemination in *S100a9*$^{-/-}$ (Fig. 5 *D–F*) or *Lcn2*$^{-/-}$ (Fig. 5 *G–I*) mice, revealing that CP and LCN2 are required for antibiotic-induced susceptibility to *A. baumannii* pneumonia.

CP, comprised of a heterodimer of S100A8 and S100A9, exerts its antimicrobial activity by binding to and sequestering zinc, manganese, nickel, and iron (67–69), while LCN2 restricts bacterial access to iron by binding siderophore molecules and preventing their uptake (70, 71). However, *A. baumannii* is able to combat these and other nutritional immunity responses via the use of the high-affinity metal uptake systems, including the zinc uptake system ZnuABC (65, 72), and through the secretion of siderophores, which are small molecules that bind iron with high affinity (73). We therefore hypothesized that during infection of antibiotic-treated mice, decreased expression of *S100a9*, *Lcn2,* and other nutritional immunity factors in neutrophils may allow for increased iron and zinc bioavailability and decreased bacterial dependence on high-affinity metal uptake systems. To assess the impact of antibiotic treatment on nutrient metal bioavailability during pneumonia, the virulence of an *A. baumannii* strain deficient in the uptake of zinc and iron was measured in both control and antibiotic treatment groups. Consistent with previous observations (72, 73), we found that *znuA,* encoding the ATPase of the ZnuABC zinc uptake system, and *bauA,* encoding the transporter of the acinetobactin siderophore, both support growth in metal-restricted media (*SI Appendix*, Fig. S7 *A–C*) and are required to compete against WT bacteria during infection (Fig. 5 *J–L*), indicating that access to iron and zinc is restricted during pneumonia. However, the competitive index (C.I.) of a Δ*znuA*Δ*bauA* mutant strain, as compared to wildtype (WT), was partially rescued in mice that received antibiotics prior to infection (Fig. 5 *J–L*), revealing that a healthy microbiota is required to limit access of *A. baumannii* to nutrient metals, including iron and zinc, during respiratory infection. Together, these results support a model in which neutrophils recruited to the lungs of antibiotic-treated mice exhibit reduced activation of nutritional immunity pathways, allowing for increased bioavailability of nutrient metals and enhanced *A. baumannii* replication and dissemination.

Discussion

Antimicrobial treatment is a major risk factor for the development of healthcare-associated infections, including infections with the emerging multidrug-resistant pathogen *A. baumannii* (33–41). In this work, we further substantiate these clinical observations in a human patient cohort and, using a murine model, demonstrate a causal link between antibiotic administration and pneumonia severity driven by dysbiosis of the gut microbiota. Finally, we demonstrate that antibiotic treatment impairs the expression of multiple arms of neutrophil-mediated effector functions in mice, including the ability to restrict *A. baumannii* access to nutrient metals via the elaboration of nutritional immunity.

The observation that reconstitution of a healthy microbiota by FMT restores the ability of antibiotic-treated mice to control bloodstream dissemination of *A. baumannii* fits within the emerging framework of a gut–lung axis, wherein microbes comprising the intestinal microbiota play significant roles in influencing immune cell development, homeostasis, and effector functions in the lung (74). Connections between dysbiosis of the intestinal microbiota and dysregulated lung immune functions have been demonstrated in the context of several chronic lung disease states, including asthma and chronic obstructive pulmonary disease (COPD) (75–78). Additionally, several studies have shown a protective role for the intestinal microbiota in controlling resistance to bacterial and viral pathogens during respiratory infection (24, 26–28, 79–81). Here, we demonstrate that microbiota disruption by antibiotics suppresses transcriptional programs governing phagocytosis, reactive oxygen species production, and nutritional immunity in the lungs of infected mice and show that this impaired immune cell function is not explained by differences in myeloid cell recruitment, but by diminished expression of effector pathways in recruited cells. While the precise mechanisms contributing to immune suppression in our antibiotic treatment model are not known, these findings are consistent with recent reports that microbiota-derived factors, including metabolites and cell envelope structural components, can systemically prime the maturation, aging, development, and activation of circulating myeloid cells, including neutrophils and monocytes (29, 30, 79, 82–84). We therefore propose a model in which antibiotic-mediated dysbiosis of the gut microbiota leads to a loss or dysregulation of microbial-derived products, resulting in altered myeloid cell development or baseline activation state prior to lung recruitment. This dysregulation in myeloid cell development or priming may then impair the ability of neutrophils and monocytes to control *A. baumannii* replication and bloodstream dissemination during respiratory infection. Future work will be targeted at addressing this hypothesis by defining the microbiota-derived factors that promote control of *A. baumannii* pneumonia and determining the mechanisms by which these factors influence the development and priming of myeloid cells prior to their lung recruitment.

Using a series of individual and combinatorial antibiotic treatment regimens, we observed that administration of vancomycin is sufficient to drive susceptibility to *A. baumannii* pneumonia and results in enhanced bloodstream dissemination. This observation is particularly striking, as vancomycin has been frequently used to treat gram-positive infections in hospitalized patients, though current guidelines emphasize stewardship and prudent use in its administration (85–87). Notably, vancomycin has limited systemic absorption after oral administration, implying that its effects after oral delivery are limited to the intestinal compartment (88, 89). Prior studies have shown that oral administration of vancomycin profoundly alters gut microbial communities by depleting obligate anaerobic taxa, including members of the Bacteroidales order, while permitting the expansion of facultative anaerobes such as *Enterobacteriaceae* (90, 91). Our work confirms these shifts and further demonstrates that *Enterobacteriaceae* enrichment correlates with higher *A. baumannii* burdens in the lung and systemic tissue sites (Fig. 3 *K* and *L*). These findings are consistent with a recent human ICU cohort study, which observed an enrichment of *Enterobacteriaceae* in patient fecal samples that was associated with critical illness and nosocomial infections at

Downloaded from https://www.pnas.org by TU DELFT BIBLIOTHEEK on October 22, 2026 from IP address 131.180.130.24.

extraintestinal tissue sites (15). Moreover, this report observed a negative correlation between fecal *Enterobacteriaceae* abundance and neutrophil maturity in human donors that was marked by hypofunctional neutrophil responses, including decreased production of neutrophil extracellular traps (15). These findings are consistent with our observations of reduced expression of neutrophil effector pathways following antibiotic administration, and, together, suggest that expansion of *Enterobacteriaceae* in the gut may have a distinct influence on microbiota-immune crosstalk and control of systemic infection.

A limitation of our antibiotic-treatment model is that antibiotics were administered orally in the drinking water, whereas many antibiotics administered in ICUs, including vancomycin, are frequently delivered intravenously. Intravenous vancomycin has limited exposure to the intestinal lumen (89), which therefore prevents direct comparison to our oral treatment model. However, oral vancomycin is also used to treat hospitalized patients, particularly those with recurrent episodes of *Clostridioides difficile* infection (92, 93), and this treatment has been associated with microbiota dysbiosis (94). Additionally, intravenous administration of other classes of antibiotics has been shown to disrupt gut microbiota composition in both human patients and rodent models (95, 96). Moreover, ICU patients receiving antibiotic treatment frequently experience profound microbiota dysbiosis, which can include expansion of *Enterobacteriaceae* (15–18). Thus, while the dosing and delivery of antibiotics in our model may differ from clinical administration, the profound microbiota dysbiosis observed in our study appears to reflect that of hospital patient populations receiving antimicrobial therapy.

While FMT restored control of bacterial dissemination from the lungs to the liver and spleen, we did not detect a restoration in control of lung colony-forming units (CFUs) after microbiota transplant, suggesting that additional, microbiota-independent factors might also be contributing to restriction of bacterial replication within this tissue site. Previous studies have reported that oral antibiotic administration in murine models can have microbiota-independent effects on control of systemic infections with a number of healthcare-associated bacterial pathogens, including *A. baumannii* (48, 49). In these reports, microbiota-independent phenotypes are driven by immune suppression caused by dehydration and malnutrition that occur during oral antibiotic administration. Consistent with these studies, we observed weight loss in mice after antibiotic treatment that was sustained even after FMT.

Our findings demonstrate that nutritional immunity constitutes a critical microbiota-dependent defense against *A. baumannii* pneumonia. Previous studies have identified lipocalin-2 and calprotectin as key effectors restricting bacterial access to iron, manganese, and zinc during *A. baumannii* infection (64–66). Here, we show that antibiotic treatment reduces neutrophil expression of these factors, and that their loss prevents the effects of antibiotics in a murine pneumonia model. One limitation of the experiments performed with *S100a9*$^{-/-}$ and *Lcn2*$^{-/-}$ mice is the potential for genotype-dependent microbiota differences in these animals. Although cohousing was employed to equilibrate microbial communities across genotypes, it has been reported that host genetic factors can continue to influence the microbiota community structure in ways that may not be fully normalized through this approach (97). However, we additionally found that the virulence of a mutant lacking high-affinity zinc and iron uptake systems is partially rescued in antibiotic-treated mice, supporting the hypothesis that microbiota disruption suppresses nutritional immunity, thereby altering pathogen access to these nutrient metals. The sequestration of nutrient metals represents a key component of the innate immune defense against numerous pathogens that cause respiratory and bloodstream infections (62); thus, our findings may extend to understanding how antibiotic exposure and microbiota disruption influence susceptibility to a broad range of healthcare-associated infections.

In summary, this work demonstrates that antibiotic-mediated dysbiosis of the intestinal microbiota drives susceptibility to *A. baumannii* pneumonia and reveals a critical role for the microbiota in regulating the expression of nutritional immunity responses employed by neutrophils to control pulmonary infection with this pathogen. These findings highlight a mechanism underlying the well-documented association between antibiotic exposure and nosocomial *A. baumannii* infections and suggest that preserving or restoring microbiota-dependent immune priming may represent a promising approach for preventing nosocomial infections with this pathogen.

Materials and Methods

The complete *Materials and Methods* can be found in *SI Appendix*.

Multistudy Cohort Integration and Taxonomic Profiling of Preinfection Fecal Microbiomes. Fecal microbiome data were integrated from several previously published prospective observational cohort studies conducted at the UCM Center that collectively profiled the gut microbiome and fecal metabolome of hospitalized patients and healthy control participants [see *SI Appendix* for detailed cohort descriptions, exclusion criteria, and Institutional Review Board (IRB) approvals] (16, 42–47). All studies were approved by the IRBs at the University of Chicago, and all participants provided informed consent prior to enrollment.

Stool samples were collected and processed using standardized protocols and profiled by shotgun metagenomic sequencing with taxonomic assignments made using MetaPhlAn4, as previously described in the originating studies. Clinical metadata, including antibiotic treatment history and dates and anatomical sites of *Acinetobacter*-positive cultures, were obtained from electronic medical records (see *SI Appendix* for data extraction and validation procedures). Infection was defined by a positive *Acinetobacter* culture with clinician-directed antibiotic treatment (see *SI Appendix* for detailed infection adjudication criteria). Fecal samples collected prior to *Acinetobacter* infection were identified through temporal alignment of microbiome sampling with antibiotic exposure and clinical culture data (see *SI Appendix* for timeline construction and sample inclusion criteria). Microbial community composition in these samples was compared to that of healthy, nonantibiotic-treated controls. Relative abundance profiles were used to assess alpha diversity (Shannon index) and beta diversity (Bray–Curtis dissimilarity with principal coordinate analysis) in R as described in *SI Appendix*.

Bacterial Strains and Culture Conditions. The strains used in this study are described in *SI Appendix*, Table S1. Strains were cultured in lysogeny broth (LB) or on LB agar plates at 37 °C.

Animal Experiments. WT C57BL/6J mice were purchased from Jackson Laboratories (stock no. 000664). *S100a9*$^{-/-}$ and *Lcn2*$^{-/-}$ mice (in a C57BL/6J background) were maintained in an animal colony at Vanderbilt University Medical Center (VUMC). A mix of male and female mice was used in experiments comparing *S100a9*$^{-/-}$ and *Lcn2*$^{-/-}$ mice with sex-matched WT C57BL/6J controls. For these experiments, mice were cohoused with sex- and age-matched WT controls for a period of 4 wk prior to antibiotic administration. Female mice were used for all other experiments. Infections were performed using 8- to 12-wk-old mice. Animals were maintained at the VUMC Animal Facility, with a 12 h light–dark cycle and food and water provided ad libitum. All animal experiments were approved and performed in compliance with the Institutional Animal Care and Use Committee (IACUC) of Vanderbilt University.

Antibiotic Administration. Mice were administered ampicillin (Sigma; 0.5 mg/mL), vancomycin (Fresenius Kabi; 0.5 mg/mL), and gentamicin (Sigma; 1.0 mg/mL) individually or in combination in their drinking water for 5 d. After termination of antibiotic treatment, normal drinking water was provided, and mice were given 2 d of recovery prior to *A. baumannii* infection.

Downloaded from https://www.pnas.org by TU DELFT BIBLIOTHEEK on October 22, 2026 from IP address 131.180.130.24.

***A. baumannii* Mouse Infections.** Mid-exponential phase cultures of *A. baumannii* were washed and resuspended in PBS at 1×10^{10} CFU/mL. Prior to infections, mice were anesthetized by intraperitoneal injection of 2,2,2 tribromoethanol diluted in PBS. Anesthetized mice were infected intranasally with 4×10^8 CFU in a 40 μL volume. Infections proceeded for 36 h, during which time survival was monitored. Mice were killed by CO_2 inhalation, and tissues were sterilely harvested and homogenized. Bacterial burdens were enumerated by plating serial dilutions onto LB agar. For competitive infections, dilutions were plated onto both LB agar and LB agar supplemented with kanamycin (Km) at 40 μg/mL to quantify each population. C.I. was determined by dividing the ratio of Km^S/Km^R bacteria in the output to the input ratio.

FMT. Mice were administered control water or antibiotic-supplemented water for 5 d. 48 h after cessation of antibiotic administration, fecal pellets were collected from mice receiving control water throughout the course of treatment. Fecal pellets were resuspended in PBS and 100 μL of the resulting fecal preparation was administered to mice in control and antibiotic treatment groups via oral gavage. As a vehicle control, additional groups of control and antibiotic-treated mice received 100 μL of PBS by oral gavage. Two days were allowed for microbiota engraftment prior to *A. baumannii* intranasal infection.

Bacterial Strain Generation. The strains and primers used in this study are listed in *SI Appendix*, Tables S1 and S2, respectively (*SI Appendix*). The Δ*znuA*Δ*bauA* mutant was created via allelic exchange as described in *SI Appendix*. Briefly, the Δ*znuA*-pFLp2 and Δ*bauA*-pFLp2 plasmids were introduced into parental strains by conjugation and integrated into the chromosome by homologous recombination. Strains harboring integrated plasmids were propagated on LB agar to allow for a second round of homologous recombination. A sucrose counterselection was then applied to select for strains that resolved the integrated plasmid. Deletion mutants were identified and confirmed as described in *SI Appendix*.

Histopathology and Immunohistochemistry (IHC). Mouse lungs were insufflated, fixed in 10% neutral buffered formalin, paraffin-embedded, and sectioned for analysis as described in *SI Appendix*. Sections were stained with hematoxylin and eosin (H&E), then assessed and scored by a board-certified veterinary pathologist (T.S.Y.) who was blinded to the experimental groups (see *SI Appendix* for a detailed scoring rubric). For IHC, slides were processed using the Leica Bond Max/RX IHC staining platform and incubated with an anti-Ly6G (cat#NBP1-00691, Novus, Littleton, CO) primary antibody, followed by incubation with a rabbit anti-rat secondary antibody (BA-4001, Vector Laboratories, Inc.). All completed slides were scanned with a 3DHISTECH Pannoramic 250 Scanner (Epredia, Kalamazoo, MI). The whole-slide images were then analyzed for the percentage of positive cells (number of positive cells/total cells detected) within the pulmonary parenchyma using QuPath v0.6.0 (98).

16S rRNA gene Sequencing and Microbiota Analysis. Fresh fecal samples were collected from individual mice prior to antibiotic administration and immediately prior to infection and frozen for storage at −20° C. DNA was isolated from fecal samples using the PowerSoil DNA isolation kit (MO BIO Laboratories). For each sample, the V4 region of the 16S rRNA gene was amplified and sequenced using the Illumina MiSeq Personal Sequencing platform. Sequence processing, taxonomic assignments, diversity analyses, and community composition profiling were performed using QIIME2 (version 2022.2), as described in *SI Appendix*.

scRNA-seq. Mice were killedat 36 hours postinfection (h.p.i.), and lungs were sterilely collected. Single-cell lung suspensions were prepared as described in *SI Appendix*. Lung suspensions were counted, blocked, and stained with anti-CD45 (BD Biosciences, 559864, 1:200) and anti-Ter119 (BioLegend, 116211, 1:200) antibodies, with fluorescence minus-one and single-color controls prepared in the same manner. Cells from individual mice (four mice per group) were multiplexed using hashing oligonucleotides, stained with a viability dye, and sorted by FACS to isolate $CD45^+Ter119^-$ and $CD45^-Ter119^-$ cell populations (see *SI Appendix* for sorting criteria).

scRNA-seq libraries were generated using the 10× Chromium 5′ platform (10× Genomics) and sequenced on an Illumina NovaSeq 6000. Reads were processed using CellRanger Count v6.1.2 (10× Genomics), quality filtered, and aligned onto the mm10 reference genome. Ambient background RNA was filtered with SoupX 1.6.1 (99) as described previously (100), and quality filtering was applied to remove low-quality cells based on mitochondrial transcript content and gene detection thresholds (see *SI Appendix* for detailed ambient RNA and quality filtering criteria).

scRNA-seq Analysis. Downstream analysis was performed in R using Seurat v4.1.1 and SCTransform v0.3.3 (101, 102). SCTransform was run with each sequencing reaction as a batch variable, and with the percentage of mitochondrial RNA as a regression variable. Following PCA, Harmony v1.2.0 was run using a theta = 1 for batch correction (103). Following an in silico sort of the *Ptprc*+ immune cells, neighbors and uniform manifold approximation and projection (UMAP) embedding were calculated on 25 dimensions of the resulting dimension reduction, and cells were assigned clusters with resolution = 1. Cellular clusters were annotated using marker genes. Marker gene expression for each cell type was calculated using a Wilcoxon test and differential gene expression between experimental conditions was assessed using MAST (104). Data visualization was performed using ggplot2, and all parts of the analysis were run in R 4.1.2.

Gr-1$^+$ Cell Depletion. Mice were intraperitoneally injected with 250 μg anti-Gr-1 monoclonal antibody, clone RB6-8C5, or with a mock PBS control. Antibodies were diluted in sterile PBS (Corning, Corning NY) and administered 24 h prior to infection and daily throughout infection. Intranasal infections of antibody and mock-treated mice were performed as described above, using a 10-fold lower inoculum of 4×10^7 CFU.

Bone Marrow Neutrophil Assays. Single-cell suspensions of bone marrow were prepared from the tibias and femurs of mice having received water supplemented with vancomycin, gentamicin, and ampicillin, or control water, for 5 d, followed by 2 d of control water. Polymorphonuclear granulocytes were isolated from bone marrow by density centrifugation to obtain neutrophils at the interface between layers of Histopaque 1119 and Histopaque 1077. Mid-exponential phase bacterial cultures were washed, normalized by optical density, opsonized in DMEM supplemented with 50% FBS, then added to neutrophils at a multiplicity of infection (MOI) of 0.025 (2,500 CFU per 100,000 neutrophils). As a control, bacteria were also applied to an equivalent volume of DMEM + 10% heat-inactivated FBS without neutrophils and incubated under the same conditions. After 2 h of incubation at 37 °C in 5% CO_2, 0.1% Triton was applied to lyse cells, then bacteria were serially diluted and plated onto LB agar to enumerate CFUs. Percentage of surviving bacteria was determined by normalizing CFUs recovered in the presence of neutrophils relative to CFUs recovered in the media-only control.

Data, Materials, and Software Availability. Specific parameter settings, a complete collection of all package versions, and code for all steps of the analysis is available at https://github.com/SucreLab/LungAcinetobacterAntibiotics (105). Raw sequencing files associated with 16S rRNA gene sequencing and metagenomic sequencing have been uploaded to the NCBI sequence read archive (SRA) with the following accessions: 16S rRNA gene sequencing: NCBI BioProject PRJNA1363572 (106); metagenomic sequencing from human donors: NCBI BioProjects PRJNA1134172 (107), PRJNA845905 (108), and PRJNA838648 (109). Raw sequencing files associated with scRNA-seq data have been uploaded to the Gene Expression Omnibus under the accession GSE313334 (110). All other data are included in the manuscript and/or supporting information.

ACKNOWLEDGMENTS. We thank members of the Skaar Laboratory for critical feedback during the assembly of this manuscript. We thank the VUMC Digital Histology Shared Resource (DHSR) for imaging of RNA FISH staining. This work was supported by the following NIH grants: R01 AI101171 and R01 AI138581 to E.P.S., K22 AI166265 to E.R.G., R01 HL168556 and K08 HL143051 to J.M.S.S., R35 GM146969 to S.H.L., R35 GM138369 to J.P.Z., and R01 DK131104 and 1R01 AI168302 to M.X.B. T32 HL094296 supported E.R.G., T32 GM150375 supported T.H.B., T32 ES007028 supported N.G.S., and T32 GM008554 supported K.A.T. R01 AI138581, R01 AG078803, and U54 DK134302 supported F.A.M. and R.V.d.P. Additional funding was provided by the Advanced Research Projects Agency for Health agreement 1AY2AX000077 to E.P.S., by the Ernest W. Goodpasture professorship to E.P.S., and by the Francis Family Foundation to J.M.S.S. and N.M.N. M.X.B. is a Howard Hughes Medical Institute Freeman Hrabowski Scholar and received additional funding from the Pew Charitable Trusts (2022-A-19568) and the Burroughs Wellcome Fund (022792). N.G.S. was supported by the Howard Hughes Medical Institute Gilliam Fellowship (GT15104) and V.M.R.R.

Downloaded from https://www.pnas.org by TU DELFT BIBLIOTHEEK on October 22, 2026 from IP address 131.180.130.24.

was supported by the Howard Hughes Medical Institute as a HHMI Hanna-Gray Fellow. We acknowledge the use of Claude Sonnet 4.6 and Grammarly for minor proofreading and editing support.

Author affiliations: [a]Department of Microbiology, University of Chicago, Chicago, IL 60637; [b]Department of Pediatrics, Vanderbilt University Medical Center, Nashville, TN 37232; [c]Biodevelopmental Origins of Lung Disease Center, Vanderbilt University School of Medicine, Nashville, TN 37232; [d]Duchossois Family Institute, University of Chicago, Chicago, IL 60637; [e]Department of Pathology, Microbiology and Immunology, Vanderbilt University Medical Center, Nashville, TN 37232; [f]Vanderbilt Institute for Infection, Immunology and Inflammation, Vanderbilt University Medical Center, Nashville, TN 37232; [g]Division of Protective Immunity, Children's Hospital of Philadelphia, Philadelphia, PA 19104; [h]Department of Pathology and Laboratory Medicine, Perelman School of Medicine, University of Pennsylvania, Philadelphia, PA 19104; [i]Delft Center for Systems and Control, Delft University of Technology, Delft, Zuid-Holland 2628 CD, The Netherlands; [j]Department of Medicine, Section of Infectious Disease and Global Health, University of Chicago Medicine, Chicago, IL 60637; [k]HHMI, Vanderbilt University Medical Center, Nashville, TN 37232; [l]Mass Spectrometry Research Center, Vanderbilt University, Nashville, TN 37232; [m]Department of Biochemistry, Vanderbilt University, Nashville, TN 37232; [n]The Center for Microbial Medicine, Children's Hospital of Philadelphia, Philadelphia, PA 19104; and [o]Department of Cell and Developmental Biology, Vanderbilt University, Nashville, TN 37232

Author contributions: E.R.G., N.M.N., J.M.S.S., and E.P.S. designed research; E.R.G., N.M.N., T.H.B., N.G.S., S.L.D., K.A.T., and V.M.R.R. performed research; F.A.M. and R.V.d.P. contributed new reagents/analytic tools; E.R.G., N.M.N., T.H.B., N.G.S., F.A.M., T.S.Y., C.J.L., M.X.B., R.V.d.P., J.P.Z., S.H.L., and J.M.S.S. analyzed data; and E.R.G. and E.P.S. wrote the paper.

1. S. Mohd Sazlly Lim *et al.*, The global prevalence of multidrug-resistance among *Acinetobacter baumannii* causing hospital-acquired and ventilator-associated pneumonia and its associated mortality: A systematic review and meta-analysis. *J. Infect.* **79**, 593–600 (2019), 10.1016/j.jinf.2019.09.012.
2. GBD 2019 Antimicrobial Resistance Collaborators, Global mortality associated with 33 bacterial pathogens in 2019: A systematic analysis for the Global Burden of Disease Study 2019. *Lancet* **400**, 2221–2248 (2022), 10.1016/S0140-6736(22)02185-7.
3. Antimicrobial Resistance Collaborators, Global burden of bacterial antimicrobial resistance in 2019: A systematic analysis. *Lancet* **399**, 629–655 (2019), 10.1016/S0140-6736(21)02724-0.
4. E. R. Green *et al.*, Bacterial hydrophilins promote pathogen desiccation tolerance. *Cell Host Microbe* **30**, 975–987.e7 (2022), 10.1016/j.chom.2022.03.019.
5. C. Dexter, G. L. Murray, I. T. Paulsen, A. Y. Peleg, Community-acquired *Acinetobacter baumannii*: Clinical characteristics, epidemiology and pathogenesis. *Expert Rev. Anti Infect. Ther.* **13**, 567–573 (2015), 10.1586/14787210.2015.1025055.
6. M. E. Falagas, E. A. Karveli, I. Kelesidis, T. Kelesidis, Community-acquired Acinetobacter infections. *Eur. J. Clin. Microbiol. Infect. Dis.* **26**, 857–868 (2007), 10.1007/s10096-007-0365-6.
7. D. Koulenti, E. Tsigou, J. Rello, Nosocomial pneumonia in 27 ICUs in Europe: Perspectives from the EU-VAP/CAP study. *Eur. J. Clin. Microbiol. Infect. Dis.* **36**, 1999–2006 (2017), 10.1007/s10096-016-2703-z.
8. D. Wong *et al.*, Clinical and pathophysiological overview of *Acinetobacter* infections: A century of challenges. *Clin. Microbiol. Rev.* **30**, 409–447 (2017), 10.1128/CMR.00058-16.
9. L. Dijkshoorn, A. Nemec, H. Seifert, An increasing threat in hospitals: Multidrug-resistant *Acinetobacter baumannii*. *Nat. Rev. Microbiol.* **5**, 939–951 (2007), 10.1038/nrmicro1789.
10. M. E. Falagas, E. A. Karveli, I. I. Siempos, K. Z. Vardakas, *Acinetobacter* infections: A growing threat for critically ill patients. *Epidemiol. Infect.* **136**, 1009–1019 (2008), 10.1017/S0950268807009478.
11. R. Cusack, E. Little, I. Martin-Loeches, Practical lessons on antimicrobial therapy for critically Ill patients. *Antibiotics* **13**, 162 (2024), 10.3390/antibiotics13020162.
12. P. Zarb *et al.*, The European Centre for Disease Prevention and Control (ECDC) pilot point prevalence survey of healthcare-associated infections and antimicrobial use. *Euro Surveill.* **17**, 20316 (2012), 10.2807/ese.17.46.20316-en.
13. J.-L. Vincent *et al.*, International study of the prevalence and outcomes of infection in intensive care units. *JAMA* **302**, 2323–2329 (2009), 10.1001/jama.2009.1754.
14. J.-F. Timsit *et al.*, Antibiotic therapy for severe bacterial infections. *Intensive Care Med.* **51**, 1867–1885 (2025), 10.1007/s00134-025-08063-0.
15. J. Schlechte *et al.*, Dysbiosis of a microbiota–immune metasystem in critical illness is associated with nosocomial infections. *Nat. Med.* **29**, 1017–1027 (2023), 10.1038/s41591-023-02243-5.
16. A. P. de Porto *et al.*, Fecal metabolite profiling identifies critically ill patients with increased 30-day mortality. *Sci. Adv.* **11**, eadt1466 (2025), 10.1126/sciadv.adt1466.
17. H. Wozniak *et al.*, Early reduction in gut microbiota diversity in critically ill patients is associated with mortality. *Ann. Intensive Care* **14**, 174 (2024), 10.1186/s13613-024-01407-x.
18. G. M. Agudelo-Ochoa *et al.*, Gut microbiota profiles in critically ill patients, potential biomarkers and risk variables for sepsis. *Gut Microbes* **12**, 1707610 (2020), 10.1080/19490976.2019.1707610.
19. M. J. Ray *et al.*, Influence of antibiotic exposure intensity on the risk of *Clostridioides difficile* infection. *Clin. Infect. Dis.* **79**, 1129–1135 (2024), 10.1093/cid/ciae259.
20. C. Ubeda *et al.*, Vancomycin-resistant *Enterococcus* domination of intestinal microbiota is enabled by antibiotic treatment in mice and precedes bloodstream invasion in humans. *J. Clin. Invest.* **120**, 4332–4341 (2010), 10.1172/JCI43918.
21. T. Shimasaki *et al.*, Increased relative abundance of *Klebsiella pneumoniae* carbapenemase-producing *Klebsiella pneumoniae* within the gut microbiota is associated with risk of bloodstream infection in long-term acute care hospital patients. *Clin. Infect. Dis.* **68**, 2053–2059 (2019), 10.1093/cid/ciy796.
22. G. Caballero-Flores, J. M. Pickard, G. Núñez, Microbiota-mediated colonization resistance: Mechanisms and regulation. *Nat. Rev. Microbiol.* **21**, 347–360 (2023), 10.1038/s41579-022-00833-7.
23. T. J. Schuijt, T. van der Poll, W. M. de Vos, W. J. Wiersinga, The intestinal microbiota and host immune interactions in the critically ill. *Trends Microbiol.* **21**, 221–229 (2013), 10.1016/j.tim.2013.02.001.
24. T. Ichinohe *et al.*, Microbiota regulates immune defense against respiratory tract influenza A virus infection. *Proc. Natl. Acad. Sci. U.S.A.* **108**, 5354–5359 (2011), 10.1073/pnas.1019378108.
25. M. A. Aufiero, T. M. Hohl, Antibiotic-induced microbiota disruption impairs neutrophil-mediated immunity to respiratory Aspergillus fumigatus infection in mice. *mBio*, e03982-25 (2026), 10.1128/mbio.03982-25.
26. T. J. Schuijt *et al.*, The gut microbiota plays a protective role in the host defence against pneumococcal pneumonia. *Gut* **65**, 575–583 (2016), 10.1136/gutjnl-2015-309728.
27. O. H. Robak *et al.*, Antibiotic treatment-induced secondary IgA deficiency enhances susceptibility to *Pseudomonas aeruginosa* pneumonia. *J. Clin. Invest.* **128**, 3535–3545 (2018), 10.1172/JCI97065.
28. R. L. Brown, R. P. Sequeira, T. B. Clarke, The microbiota protects against respiratory infection via GM-CSF signaling. *Nat. Commun.* **8**, 1512 (2017), 10.1038/s41467-017-01803-x.
29. H. S. Deshmukh *et al.*, The microbiota regulates neutrophil homeostasis and host resistance to *Escherichia coli* K1 sepsis in neonatal mice. *Nat. Med.* **20**, 524–530 (2014), 10.1038/nm.3542.
30. T. B. Clarke *et al.*, Recognition of peptidoglycan from the microbiota by Nod1 enhances systemic innate immunity. *Nat. Med.* **16**, 228–231 (2010), 10.1038/nm.2087.
31. B. McDonald *et al.*, Programing of an intravascular immune firewall by the gut microbiota protects against pathogen dissemination during infection. *Cell Host Microbe* **28**, 660–668.e4 (2020), 10.1016/j.chom.2020.07.014.
32. E. Montaldo *et al.*, Cellular and transcriptional dynamics of human neutrophils at steady state and upon stress. *Nat. Immunol.* **23**, 1470–1483 (2022), 10.1038/s41590-022-01311-1.
33. J.-L. García-Garmendia *et al.*, Risk factors for *Acinetobacter baumannii* nosocomial bacteremia in critically Ill patients: A cohort study. *Clin. Infect. Dis.* **33**, 939–946 (2001), 10.1086/322584.
34. A. Čiginskienė, A. Dambrauskienė, J. Rello, D. Adukauskienė, Ventilator-associated pneumonia due to drug-resistant Acinetobacter baumannii: Risk factors and mortality relation with resistance profiles, and independent predictors of in-hospital mortality. *Medicina (Kaunas)* **55**, 49 (2019), 10.3390/medicina55020049.
35. J. Y. Jung *et al.*, Risk factors for multi-drug resistant *Acinetobacter baumannii* bacteremia in patients with colonization in the intensive care unit. *BMC Infect. Dis.* **10**, 228 (2010), 10.1186/1471-2334-10-228.
36. S. Corcione *et al.*, Risk factors for mortality in *Acinetobacter baumannii* bloodstream infections and development of a predictive mortality model. *J. Glob. Antimicrob. Resist.* **38**, 317–326 (2024), 10.1016/j.jgar.2024.06.010.
37. M. R. De Blasiis *et al.*, Impact of antibiotic exposure on antibiotic-resistant *Acinetobacter baumannii* isolation in intensive care unit patients: A systematic review and meta-analysis. *J. Hosp. Infect.* **143**, 123–139 (2024), 10.1016/j.jhin.2023.11.002.
38. J. Inchai *et al.*, Risk factors of multidrug-resistant, extensively drug-resistant and pandrug-resistant *Acinetobacter baumannii* ventilator-associated pneumonia in a Medical Intensive Care Unit of University Hospital in Thailand. *J. Infect. Chemother.* **21**, 570–574 (2015), 10.1016/j.jiac.2015.04.010.
39. E. S. Özgür *et al.*, Ventilator-associated pneumonia due to extensive drug-resistant *Acinetobacter baumannii*: Risk factors, clinical features, and outcomes. *Am. J. Infect. Control* **42**, 206–208 (2014), 10.1016/j.ajic.2013.09.003.
40. H.-C. Chang *et al.*, Mortality risk factors in patients with *Acinetobacter baumannii* ventilator-associated pneumonia. *J. Formos. Med. Assoc.* **110**, 564–571 (2011), 10.1016/j.jfma.2011.07.004.
41. E. G. Playford, J. C. Craig, J. R. Iredell, Carbapenem-resistant *Acinetobacter baumannii* in intensive care unit patients: Risk factors for acquisition, infection and their consequences. *J. Hosp. Infect.* **65**, 204–211 (2007), 10.1016/j.jhin.2006.11.010.
42. C. J. Lehmann *et al.*, Fecal metabolite profiling identifies liver transplant recipients at risk for postoperative infection. *Cell Host Microbe* **32**, 117–130.e4 (2024), 10.1016/j.chom.2023.11.016.
43. M. A. Odenwald *et al.*, Bifidobacteria metabolize lactulose to optimize gut metabolites and prevent systemic infection in patients with liver disease. *Nat. Microbiol.* **8**, 2033–2049 (2023), 10.1038/s41564-023-01493-w.
44. M. A. Odenwald *et al.*, Fecal butyrate and deoxycholic acid concentrations correlate with mortality in patients with liver disease. *Gastro Hep Adv.* **4**, 100695 (2025), 10.1016/j.gastha.2025.100695.
45. M. R. Stutz *et al.*, Immunomodulatory fecal metabolites are associated with mortality in COVID-19 patients with respiratory failure. *Nat. Commun.* **13**, 6615 (2022), 10.1038/s41467-022-34260-2.
46. M. Dela Cruz *et al.*, Reduced immunomodulatory metabolite concentrations in peri-transplant fecal samples from heart allograft recipients. *Front. Transplant.* **2**, 1182534 (2023), 10.3389/frtra.2023.1182534.
47. A. S. Little *et al.*, Dietary- and host-derived metabolites are used by diverse gut bacteria for anaerobic respiration. *Nat. Microbiol.* **9**, 55–69 (2024), 10.1038/s41564-023-01560-2.
48. K. A. Lacey *et al.*, Microbiome-independent effects of antibiotics in a murine model of nosocomial infections. *mBio* **13**, e0124022 (2022), 10.1128/mbio.01240-22.
49. K. A. Lacey *et al.*, Dietary and water restriction leads to increased susceptibility to antimicrobial resistant pathogens. *Sci. Adv.* **10**, eadi7438 (2024), 10.1126/sciadv.adi7438.
50. J. Gray *et al.*, Intestinal commensal bacteria mediate lung mucosal immunity and promote resistance of newborn mice to infection. *Sci. Transl. Med.* **9**, eaaf9412 (2017), 10.1126/scitranslmed.aaf9412.
51. K. Honda, D. R. Littman, The microbiome in infectious disease and inflammation. *Annu. Rev. Immunol.* **30**, 759–795 (2012), 10.1146/annurev-immunol-020711-074937.
52. C. K. I. Jordan, T. B. Clarke, How does the microbiota control systemic innate immunity? *Trends Immunol.* **45**, 94–102 (2024), 10.1016/j.it.2023.12.002.
53. R. B. Panwar, R. P. Sequeira, T. B. Clarke, Microbiota-mediated protection against antibiotic-resistant pathogens. *Genes Immun.* **22**, 255–267 (2021), 10.1038/s41435-021-00129-5.
54. L. V. Hooper, D. R. Littman, A. J. Macpherson, Interactions between the microbiota and the immune system. *Science* **336**, 1268–1273 (2012), 10.1126/science.1223490.
55. L. D. Palmer *et al.*, Dietary zinc deficiency promotes *Acinetobacter baumannii* lung infection via IL-13 in mice. *Nat. Microbiol.* **9**, 3196–3209 (2024), 10.1038/s41564-024-01849-w.
56. H. van Faassen *et al.*, Neutrophils play an important role in host resistance to respiratory infection with *Acinetobacter baumannii* in mice. *Infect. Immun.* **75**, 5597–5608 (2007), 10.1128/IAI.00762-07.

Downloaded from https://www.pnas.org by TU DELFT BIBLIOTHEEK on October 22, 2026 from IP address 131.180.130.24.

57. H. H. Lee *et al.*, Depletion of alveolar macrophages increases pulmonary neutrophil infiltration, tissue damage, and sepsis in a murine model of Acinetobacter baumannii pneumonia. *Infect. Immun.* **88**, e00128-20 (2020), 10.1128/IAI.00128-20.
58. H. Qiu *et al.*, Role of macrophages in early host resistance to respiratory Acinetobacter baumannii infection. *PLoS One* **7**, e40019 (2012), 10.1371/journal.pone.0040019.
59. X. Zeng *et al.*, A lethal pneumonia model of *Acinetobacter baumannii*: An investigation in immunocompetent mice. *Clin. Microbiol. Infect.* **25**, 516.e1–516.e4 (2019), 10.1016/j.cmi.2018.12.020.
60. J. M. Daley *et al.*, Use of Ly6G-specific monoclonal antibody to deplete neutrophils in mice. *J. Leukoc. Biol.* **83**, 64–70 (2008), 10.1189/jlb.0407247.
61. M. I. Hood-Pishchany *et al.*, Broad-spectrum suppression of bacterial pneumonia by aminoglycoside-propagated Acinetobacter baumannii. *PLoS Pathog.* **16**, e1008374 (2020), 10.1371/journal.ppat.1008374.
62. C. C. Murdoch, E. P. Skaar, Nutritional immunity: The battle for nutrient metals at the host-pathogen interface. *Nat. Rev. Microbiol.* **20**, 657–670 (2022), 10.1038/s41579-022-00745-6.
63. A. J. Monteith, E. P. Skaar, The impact of metal availability on immune function during infection. *Trends Endocrinol. Metab.* **32**, 916–928 (2021), 10.1016/j.tem.2021.08.004.
64. J. R. Sheldon *et al.*, Lipocalin-2 is an essential component of the innate immune response to Acinetobacter baumannii infection. *PLoS Pathog.* **18**, e1010809 (2022), 10.1371/journal.ppat.1010809.
65. M. I. Hood *et al.*, Identification of an Acinetobacter baumannii zinc acquisition system that facilitates resistance to calprotectin-mediated zinc sequestration. *PLoS Pathog.* **8**, e1003068 (2012), 10.1371/journal.ppat.1003068.
66. L. J. Juttukonda, W. J. Chazin, E. P. Skaar, Acinetobacter baumannii coordinates urea metabolism with metal import to resist host-mediated metal limitation. *mBio* **7**, e01475-16 (2016), 10.1128/mBio.01475-16.
67. S. M. Damo *et al.*, Molecular basis for manganese sequestration by calprotectin and roles in the innate immune response to invading bacterial pathogens. *Proc. Natl. Acad. Sci. U.S.A.* **110**, 3841–3846 (2013), 10.1073/pnas.1220341110.
68. T. G. Nakashige, E. M. Zygiel, C. L. Drennan, E. M. Nolan, Nickel sequestration by the host-defense protein human calprotectin. *J. Am. Chem. Soc.* **139**, 8828–8836 (2017), 10.1021/jacs.7b01212.
69. T. G. Nakashige, B. Zhang, C. Krebs, E. M. Nolan, Human calprotectin is an iron-sequestering host-defense protein. *Nat. Chem. Biol.* **11**, 765–771 (2015), 10.1038/nchembio.1891.
70. D. H. Goetz *et al.*, The neutrophil lipocalin NGAL is a bacteriostatic agent that interferes with siderophore-mediated iron acquisition. *Mol. Cell* **10**, 1033–1043 (2002), 10.1016/s1097-2765(02)00708-6.
71. T. H. Flo *et al.*, Lipocalin 2 mediates an innate immune response to bacterial infection by sequestrating iron. *Nature* **432**, 917–921 (2004), 10.1038/nature03104.
72. L. E. Hesse, Z. R. Lonergan, W. N. Beavers, E. P. Skaar, The *Acinetobacter baumannii* Znu system overcomes host-imposed nutrient zinc limitation. *Infect. Immun.* **87**, e00746-19 (2019), 10.1128/IAI.00746-19.
73. J. R. Sheldon, E. P. Skaar, *Acinetobacter baumannii* can use multiple siderophores for iron acquisition, but only acinetobactin is required for virulence. *PLoS Pathog.* **16**, e1008995 (2020), 10.1371/journal.ppat.1008995.
74. K. F. Budden *et al.*, Emerging pathogenic links between microbiota and the gut–lung axis. *Nat. Rev. Microbiol.* **15**, 55–63 (2017), 10.1038/nrmicro.2016.142.
75. A. Trompette *et al.*, Gut microbiota metabolism of dietary fiber influences allergic airway disease and hematopoiesis. *Nat. Med.* **20**, 159–166 (2014), 10.1038/nm.3444.
76. Y. He *et al.*, Gut–lung axis: The microbial contributions and clinical implications. *Crit. Rev. Microbiol.* **43**, 81–95 (2017), 10.1080/1040841X.2016.1176988.
77. N. Li *et al.*, Gut microbiota dysbiosis contributes to the development of chronic obstructive pulmonary disease. *Respir. Res.* **22**, 274 (2021), 10.1186/s12931-021-01872-z.
78. T. P. Wypych *et al.*, Microbial metabolism of L-tyrosine protects against allergic airway inflammation. *Nat. Immunol.* **22**, 279–286 (2021), 10.1038/s41590-020-00856-3.
79. A. Trompette *et al.*, Dietary fiber confers protection against flu by shaping Ly6c-patrolling monocyte hematopoiesis and CD8+ T cell metabolism. *Immunity* **48**, 992–1005.e8 (2018), 10.1016/j.immuni.2018.04.022.
80. T. B. Clarke, Early innate immunity to bacterial infection in the lung is regulated systemically by the commensal microbiota via nod-like receptor ligands. *Infect. Immun.* **82**, 4596–4606 (2014), 10.1128/iai.02212-14.
81. L.-W. Chen, P.-H. Chen, C.-M. Hsu, Commensal microflora contribute to host defense against *Escherichia coli* pneumonia through toll-like receptors. *Shock* **36**, 67–75 (2011), 10.1097/SHK.0b013e3182184ee7.
82. D. Zhang *et al.*, Neutrophil ageing is regulated by the microbiome. *Nature* **525**, 528–532 (2015), 10.1038/nature15367.
83. L. K. Weaver *et al.*, Microbiota-dependent signals are required to sustain TLR-mediated immune responses. *JCI Insight* **4**, e124370 (2019), 10.1172/jci.insight.124370.
84. L. Möhle *et al.*, Ly6Chi monocytes provide a link between antibiotic-induced changes in gut microbiota and adult hippocampal neurogenesis. *Cell Rep.* **15**, 1945–1956 (2016), 10.1016/j.celrep.2016.04.074.
85. S. S. Magill *et al.*, Prevalence of antimicrobial use in U.S. acute care hospitals, May–September 2011. *JAMA* **312**, 1438–1446 (2014), 10.1001/jama.2014.12923.
86. S. S. Magill *et al.*, Antimicrobial use in US hospitals: Comparison of results from Emerging Infections Program prevalence surveys, 2015 and 2011. *Clin. Infect. Dis.* **72**, 1784–1792 (2021), 10.1093/cid/ciaa373.
87. M. J. Rybak *et al.*, Therapeutic monitoring of vancomycin for serious methicillin-resistant *Staphylococcus aureus* infections: A revised consensus guideline and review by the American Society of Health-System Pharmacists, the Infectious Diseases Society of America, the Pediatric Infectious Diseases Society, and the Society of Infectious Diseases Pharmacists. *Am. J. Health. Syst. Pharm.* **77**, 835–864 (2020), 10.1093/ajhp/zxaa036.
88. S. Rao *et al.*, Systemic absorption of oral vancomycin in patients with *Clostridium difficile* infection. *Scand. J. Infect. Dis.* **43**, 386–388 (2011), 10.3109/00365548.2010.544671.
89. R. C. Moellering, D. J. Krogstad, D. J. Greenblatt, Pharmacokinetics of vancomycin in normal subjects and in patients with reduced renal function. *Rev. Infect. Dis.* **3**, S230–S235 (1981).
90. V. C. Harris *et al.*, Effect of antibiotic-mediated microbiome modulation on rotavirus vaccine immunogenicity: A human, randomized-control proof-of-concept trial. *Cell Host Microbe* **24**, 197–207.e4 (2018), 10.1016/j.chom.2018.07.005.
91. S. Isaac *et al.*, Short- and long-term effects of oral vancomycin on the human intestinal microbiota. *J. Antimicrob. Chemother.* **72**, 128–136 (2017), 10.1093/jac/dkw383.
92. S. Johnson *et al.*, Clinical practice guideline by the Infectious Diseases Society of America (IDSA) and Society for Healthcare Epidemiology of America (SHEA): 2021 Focused update guidelines on management of Clostridioides difficile infection in adults. *Clin. Infect. Dis.* **73**, e1029–e1044 (2021), 10.1093/cid/ciab549.
93. J. van Prehn *et al.*, European society of clinical microbiology and infectious diseases: 2021 update on the treatment guidance document for *Clostridioides difficile* infection in adults. *Clin. Microbiol. Infect.* **27** (suppl. 2), S1–S21 (2021), 10.1016/j.cmi.2021.09.038.
94. C. Edlund, L. Barkholt, B. Olsson-Liljequist, C. E. Nord, Effect of vancomycin on intestinal flora of patients who previously received antimicrobial therapy. *Clin. Infect. Dis.* **25**, 729–732 (1997), 10.1086/513755.
95. S. A. Kelly *et al.*, Antibiotic therapy and the gut microbiome: Investigating the effect of delivery route on gut pathogens. *ACS Infect. Dis.* **7**, 1283–1296 (2021), 10.1021/acsinfecdis.1c00081.
96. A. E. Pérez-Cobas *et al.*, Gut microbiota disturbance during antibiotic therapy: A multi-omic approach. *Gut* **62**, 1591–1601 (2013), 10.1136/gutjnl-2012-303184.
97. H. B. Lietuvninkas, A. Chervonsky, T. Golovkina, Cohousing or cross-fostering followed by cohousing does not normalize the microbiomes of genetically distinct adult mice. *Cell Rep.* **44**, 116402 (2025), 10.1016/j.celrep.2025.116402.
98. P. Bankhead *et al.*, QuPath: Open source software for digital pathology image analysis. *Sci. Rep.* **7**, 16878 (2017), 10.1038/s41598-017-17204-5.
99. M. D. Young, S. Behjati, SoupX removes ambient RNA contamination from droplet-based single-cell RNA sequencing data. *Gigascience* **9**, giaa151 (2020), 10.1093/gigascience/giaa151.
100. N. M. Negretti *et al.*, A single-cell atlas of mouse lung development. *Development* **148**, dev199512 (2021), 10.1242/dev.199512.
101. Y. Hao *et al.*, Integrated analysis of multimodal single-cell data. *Cell* **184**, 3573–3587.e29 (2021), 10.1016/j.cell.2021.04.048.
102. S. Choudhary, R. Satija, Comparison and evaluation of statistical error models for scrna-seq. *Genome Biol.* **23**, 27 (2022), 10.1186/s13059-021-02584-9.
103. I. Korsunsky *et al.*, Fast, sensitive and accurate integration of single-cell data with Harmony. *Nat. Methods* **16**, 1289–1296 (2019), 10.1038/s41592-019-0619-0.
104. G. Finak *et al.*, MAST: A flexible statistical framework for assessing transcriptional changes and characterizing heterogeneity in single-cell RNA sequencing data. *Genome Biol.* **16**, 278 (2015), 10.1186/s13059-015-0844-5.
105. E. R. Green *et al.*, Code associated with "The intestinal microbiota impacts nutritional immunity and resistance to Acinetobacter baumannii pneumonia." GitHub. https://github.com/SucreLab/LungAcinetobacterAntibiotics. Deposited 10 November 2025.
106. E. R. Green *et al.*, "16S rRNA gene sequencing of antibiotic-treated mice." NCBI. https://www.ncbi.nlm.nih.gov/sra/PRJNA1363572. Deposited 13 November 2025.
107. A. P. de Porto *et al.*, "Fecal metabolite profiling identifies critically ill patients with increased 30-day mortality risk." NCBI. https://www.ncbi.nlm.nih.gov/bioproject/PRJNA1134172. Deposited 10 July 2024.
108. M. Dela Cruz *et al.*, "Gut microbiome of Heart Transplant Patients at University of Chicago Hospital." NCBI. https://www.ncbi.nlm.nih.gov/bioproject/PRJNA845905. Deposited 4 June 2022.
109. M. A. Odenwald *et al.*, "Healthy Human Stool Donors from Duchossois Family Institute at University of Chicago." NCBI. https://www.ncbi.nlm.nih.gov/bioproject/PRJNA838648. Deposited 16 May 2022.
110. E. R. Green *et al.*, scRNA-seq data from, "The intestinal microbiota impacts nutritional immunity and resistance to Acinetobacter baumannii pneumonia." NCBI. https://www.ncbi.nlm.nih.gov/geo/query/acc.cgi?acc=GSE313334. Deposited 10 December 2025.

Downloaded from https://www.pnas.org by TU DELFT BIBLIOTHEEK on October 22, 2026 from IP address 131.180.130.24.